Short Papers

Symmetry Detection by Generalized Complex (GC) Moments: A Close-Form Solution

Dinggang Shen, Horace H.S. Ip,
Kent K.T. Cheung, and Eam Khwang Teoh

Abstract—This paper presents a unified method for detecting both reflection-symmetry and rotation-symmetry of 2D images based on an identical set of features, i.e., the *first three* nonzero generalized complex (GC) moments. This method is theoretically guaranteed to detect all the axes of symmetries of *every* 2D image, if more nonzero GC moments are used in the feature set. Furthermore, we establish the relationship between reflectional symmetry and rotational symmetry in an image, which can be used to check the correctness of symmetry detection. This method has been demonstrated experimentally using more than 200 images.

Index Terms—Symmetry detection, reflectional and rotational symmetry, symmetric axis, generalized complex (GC) moments, fold number, fold axes, rotationally symmetric image, reflection-symmetric image.

1 Introduction

SYMMETRY, as one of the basic features of shapes and objects, has been studied extensively in the computer vision area. Symmetrical descriptions of shapes and the detection of symmetrical features of objects are very useful in guiding shape matching, model-based object matching and object recognition [1], [2], [3], [4]. Symmetrical information is also useful in robotics for recognition, inspection, grasping, and reasoning [5]. Usually, symmetry is considered as a binary feature, i.e., an object is either symmetric or not symmetric. For quantifying the symmetry of objects, symmetry can also be a continuous feature [7].

Rotational symmetry and reflectional symmetry are two commonly studied types of symmetries. A 2D image is said to be reflection-symmetric if it is invariant to reflection with respect to one or more straight lines, denoted as *reflection-symmetric axes*. A 2D image is said to be order K rotationally symmetric, if it is invariant under rotation of $2\pi/K$ radians about the center of mass of the image and K is the largest integer. This image is usually called rotationally symmetric image with K folds (K-RSI). The orientations of these K folds are defined in this paper by *K fold axes*. The following overview will clarify that none of the existing techniques could provide a complete solution to the problem in the sense that no algorithm yet exists for detecting all the reflection-symmetric axes and rotationally symmetric folds (or fold axes) of a 2D image.

- *D. Shen and E.K. Teoh are with the School of Electrical and Electronic Engineering, Nanyang Technological University, Singapore 639798. E-mail: {edgshen, eekteoh}@ntu.edu.sg.*
- *H.H.S. Ip and K.K.T. Cheung are with the Image Computing Group, Department of Computer Science, City University of Hong Kong, Kowloon, Hong Kong. E-mail: cship@cityu.edu.hk, ktcheung@cs.cityu.edu.hk.*

Manuscript received 16 Mar 1998; revised 29 Dec. 1998.
For information on obtaining reprints of this article, please send e-mail to: tpami@computer.org, and reference IEEECS Log Number 107637.

Much of the research literature is concerned with reflection-symmetry detection. Labonte et al. [11] considered the problem of detecting global bilateral symmetry. Zielke et al. [12] only looked at vertical or near-vertical symmetry axes in the image for car-following. Atallah [8] detected the axis of reflectional symmetry by first determining the centroid position and then using a string pattern matching technique, which considered all possible lines passing through the centroid. However, this method is only suitable for planar figures made up of segments, circles, points, etc. Marloa [6] presented an algorithm for finding the number and positions of the symmetry axes of a symmetric or almost-symmetric planar image. This technique required the evaluation of rational functions and addressed the detection of rotational symmetry. Sun [28] used orientation histograms for detecting reflection symmetry in gray-level image, but it can only detect simple bilateral symmetry.

The orientation detection methods, i.e., GPA [18], FPA [19], and UPA [20], can only determine the rotational symmetries of very *simple* objects. Pei and Lin [13] introduced a modified Fourier descriptor to determine the fold number of RSI, based on the observation that the first nonzero Fourier coefficient is located on the fundamental frequency. However, this observation is not always true for certain types of images, i.e., the *three* images shown in Fig. 1, their Fourier coefficients at their own fold number are zeros. Similar assumption was also implicitly suggested and used by Sun [17]. Lin [14] detected the fold number using a simple mathematical property. However, the detection of fold axes was not totally solved, which makes the technique unable to detect the fold axes of any of the images shown in Fig. 1.

Masuda et al. [9] described a method of extracting both rotational and reflectional symmetries by performing correlation with the rotated and reflected images. This method incurs high computational cost and memory requirements, since all possible transformations have to be tried. Sun and Sherrah [10] used the extended images for 3D symmetry detection. They formulated the symmetry detection problem as a correlation of the Gaussian image. However, different processing and representation methods were needed, respectively, for reflectional and rotational symmetry detection, which obviously increased computation. Furthermore, this method is unable to determine whether the input image is symmetric or not.

The above review clearly shows that most of the existing methods can determine *either* reflectional symmetry *or* rotational symmetry. Even for those methods which are able to detect both reflectional and rotational symmetry, they rely on different processes. Currently, there is no method which uses an identical set of features to detect these two forms of symmetries. Furthermore, no

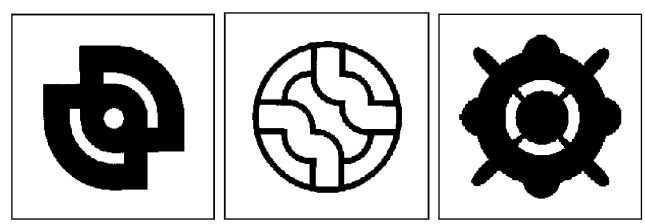

(a) (b) (c)

Fig. 1. Three images whose Fourier coefficients at their corresponding fold numbers are all zero. Fold number and the first order making Fourier coefficient nonzero are: (a) 2 and 4, (b) 2 and 6, (c) 4 and 8.

method is guaranteed to detect *all* the symmetric axes of *every* 2D image. In this paper, we have proposed a unified method of using an identical set of features, i.e., nonzero GC moments, to detect *all* reflectional and fold axes of every 2D image. In practice, all the reflection-symmetric axes and the fold axes of *almost every* image can be determined by the *first three* nonzero GC moments and the proposed method can be used for the retrieval of complex geometrical shapes such as trademark images [27].

2 Properties Concerning GC Moments of Symmetric Images

A set of nonzero GC moments forms the basis of our algorithms for detecting symmetries of every image. We first give the Fourier expansion of a general image function and the definition of GC moments, then the properties of GC moments related to reflection-symmetric images and rotationally symmetric images are presented, respectively, in Subsections 2.1 and 2.2. Also, the rules of selecting parameter p in GC moment $GC_{p,q}$ and controlling the process of detecting nonzero GC moments are given in Subsection 2.3.

The image center can be easily determined using regular moments as in [21], [22]. Let $f(x, y)$ represent a centered image. Its corresponding function in polar coordinate is $f(r, \theta)$. The pqth generalized complex (GC) moment of image function $f(r, \theta)$ is defined as

$$GC_{p,q} = R_{p,q}e^{j\varphi_{p,q}} = \frac{1}{2\pi}\int_0^{2\pi}\int_0^{\infty} f(r, \theta)(r^p e^{jq\theta})rdrd\theta,$$

where p is a nonnegative integer, and q a positive integer. GC moments have been used previously by the authors to develop new algorithms for image normalization and orientation detection [15], [16]. Complex moments in Gabor space were also used to find symmetries in [23]. The advantage of using GC moments over complex moments is that the orders p and q are independent in the definition of GC moments. Meanwhile, by using the selection rules in Subsection 2.3, different orders p can be selected for different images, including peculiar images.

Any image function $f(r, \theta)$ can be expressed through the Fourier expansion,

$$f(r, \theta) = \sum_{m=-\infty}^{\infty} f_m(r)e^{-jm\theta},$$

where

$$f_m(r) = \frac{1}{2\pi}\int_0^{2\pi} f(r, \theta)e^{jm\theta}d\theta.$$

Here, Fourier expansion is used to analyze the properties of GC moments for symmetric images.

2.1 Reflectional Symmetry

The reflection symmetric axes should pass through the center of mass of the image. Mathematically, the necessary and sufficient condition for the centered image ($f(r, \theta)$) to be reflection-symmetric is $f(r, \phi + \theta) = f(r, \phi - \theta)$, where ϕ is an angle from the x-axis to the symmetric axis. The line passing through the *origin* at an angle of ϕ is the reflection-symmetric axis of the given image.

The image with the x-axis as its reflection-symmetric axis is named here the *standard* reflection-symmetric image. It can be seen from Theorem 2.1, which is proven in the Appendix, that if all GC moments are real, then $f(r, \theta)$ is a *standard* reflectional-symmetric image. This property will be used in Section 3 to derive the technique for detecting the reflection-symmetric axes of an image.

THEOREM 2.1. *The necessary and sufficient condition for $f(r, \theta)$ reflection-symmetric about the x-axis is that all GC moments $GC_{p,q}$ must be real.*

2.2 Rotational Symmetry

For a K-RSI, its function $f(r, \theta)$ can be mathematically described by the following equation.

$$f(r, \theta) = f\left(r, \theta + \frac{(i-1)\times 2\pi}{K}\right), \quad i = 1, 2, \ldots, ; \quad \theta \in [0, 2\pi).$$

Based on this mathematical description, the corresponding Fourier expansion of a given K-RSI becomes

$$f(r, \theta) = \sum_{l=-\infty}^{\infty} f_{K\times l}(r)e^{-j(K\times l)\theta},$$

where

$$f_{K\times l}(r) = \frac{K}{2\pi}\int_0^{\frac{2\pi}{K}} f(r, \theta)e^{j(K\times l)\theta}d\theta.$$

An important observation from the Fourier expansion of a K-RSI is that, the Fourier coefficient $f_m(r)$ of K-RSI is zero if order m is not a multiple of the fold number K.

Since the relationship between the GC moment, $GC_{p,q}$, and the Fourier coefficient $f_m(r)$ is

$$GC_{p,q} = \int_0^{\infty} f_q(r)r^p rdr,$$

the property of GC moments for a K-RSI can be given in Theorem 2.2.

THEOREM 2.2. *If the given image function $f(r, \theta)$ is a K-RSI, then its corresponding GC moment $GC_{p,q}$ is zero for any q which is not a multiple of K.*

2.3 Practical Ramification: Controlling the Process of Detecting Nonzero GC Moments

The order p in GC_{pq} is usually fixed during the process of detecting nonzero GC moments. Thus, in a real application, determining an appropriate p is a key step. Also it is very important to determine whether the remaining nonzero GC moments can be detected. In the following, we give two criteria:

1) for choosing the appropriate p based on the ratio of the total alternating energy to the total energy (a_p), and
2) for controlling the process of detecting nonzero GC moments by the ratio of the residue energy to the total energy (b_q).

The detailed explanation can be found in [15].

Function $h_p(\theta)$ is 1D radial projection of the image function $f(r, \theta)$ on r^p,

$$h_p(\theta) = \int_0^{\infty} f(r, \theta)r^p rdr.$$

(Please refer to [15] for an example of the radial project function $h_p(\theta)$ for an image.) The Fourier transform of $h_p(\theta)$ is

$$H_p(q) = \frac{1}{2\pi}\int_0^{2\pi} h_p(\theta)e^{jq\theta}d\theta.$$

Then, the ratio

$$a_p = 1 - \frac{2\pi\left\|H_p(0)\right\|^2}{\int_0^{2\pi}\left[h_p(\theta)\right]^2 d\theta}$$

can be used to determine whether the 1D function $h_p(\theta)$ has a strong periodicity. In our study, we select p such that a_p is over 5 percent.

Besides, the ratio of the residue energy to the total energy is

$$b_q = 1 - \frac{2\pi\left(\left\|H_P(0)\right\|^2 + 2\sum_{m=1}^{q}\left\|H_P(m)\right\|^2\right)}{\int_0^{2\pi}\left[h_P(\theta)\right]^2 d\theta}.$$

The threshold used for b_q has been set to 1 percent in all our experiments.

3 Detection of Reflectional Symmetry Axes

3.1 Generalized Detection Method

Based on Theorem 2.1, this section will use the phases of nonzero GC moments to detect all the axes of reflectional symmetries of a 2D image. Assume that the set of the detected nonzero GC moments is $\{GC_{p,q_j},\ j = 1, 2, \ldots\}$, and the set of the corresponding phases is $\{\varphi_{p,q_j},\ j = 1, 2, \ldots\}$. If the image is a *standard* reflectional-symmetric image, then all nonzero GC moments in the set $\{GC_{p,q_j},\ j = 1, 2, \ldots\}$ must be real (positive or negative). Thus, the phase of a nonzero GC moment must be a multiple of π, i.e., $k\pi$, where k is an integer. If the *standard* reflectional-symmetric image $f(r, \theta)$ is counterclockwise rotated by an angle of β and becomes $f(r, \theta - \beta)$, then the nonzero GC moments of the rotated image $f(r, \theta - \beta)$ will become

$$\left\{GC_{p,q_j} \cdot e^{jq_j\beta}, j = 1, 2, \ldots\right\},$$

and the phase of

$$GC_{p,q_j} \cdot e^{jq_j\beta}$$

is $q_j\beta - k\pi$.

For a given image, we do not know, a priori, whether the input image is reflection-symmetric or not. And even for a reflection-symmetric image, we cannot guarantee that the x-axis is exactly its reflectional axis. For ease of discussion and without lose of generality, let's assume the input image is the rotated version, with a rotation angle β, of the *standard* reflection-symmetric image. Suppose the phase of the jth detected nonzero GC moment GC_{p,q_j} is φ_{p,q_j}. The phase φ_{p,q_j} can be represented as $\varphi_{pq_j} = q_j\beta - k\pi$. Accordingly, the line passing through the origin at an angle of β *may* be the reflection-symmetric axis of the current image. Theorem 3.1 given below defines the possible set of reflection-symmetric axes of the input image, based only on the jth nonzero GC moment. There might exist no reflection-symmetric axis at all for the input image, however, if such axes exist, it is guaranteed to be included in the set of the axes which is defined in Theorem 3.1.

It is easy to note from Theorem 3.1 that the actual reflection-symmetric axes must be contained in any set of axes which is defined by any nonzero GC moment of the input image. Theorem 3.2 gives the method of calculating all the reflection-symmetric axes by using all the nonzero GC moments.

THEOREM 3.1. *The reflection-symmetric axes of the input image $f(r, \theta)$ are included in the set of axes*

$$AxesSet_{q_j} = \left\{\text{axis with angle } \beta \middle| \beta = \frac{\varphi_{pq_j} + k\pi}{q_j},\ k = 0, 1, \ldots, (q_j - 1)\right\},$$

where φ_{pq_j} is the phase of the jth nonzero GC moment of the input image $f(r, \theta)$.

THEOREM 3.2 *All the reflection-symmetric axes of the input image $f(r, \theta)$ are included in the axes set $AxesSet$, defined by*

$$AxesSet = AxesSet_{q_1} \cap AxesSet_{q_2} \cap AxesSet_{q_3} \cap \ldots \cap AxesSet_{q_j} \cap \ldots .$$

All the axes in $AxesSet$ are potentially the reflection-symmetric axes of the input image $f(r, \theta)$.

3.2 A Practical Reflection-Symmetry Detector (PRSD)

In practice, it is impossible for us to first calculate all the nonzero GC moments and then use them to detect the reflection-symmetric axes. Similarly, when computing $A \cap B$, we should check whether both line a in set A and line b in set B have similar orientations. PRSD is summarized as follows.

PRSD: For real applications, all the reflection-symmetric axes of almost every image $f(r, \theta)$ can be determined by the first *three* nonzero moments,

$$AxesSet = AxesSet_{q_1} \cap AxesSet_{q_2} \cap AxesSet_{q_3}.$$

Notice that, only the likelihood of these elements is required when comparing elements from different sets.

We will show below that the first three nonzero GC moments are sufficient to detect all the reflection-symmetric axes of every image in our image database, which contains more than 200 images. We show that for most images, all the reflection-symmetric axes are exactly the axes in the first axes set (case 1). While for some images, only some of the axes in the first axes set are exactly the reflection-symmetric axes (case 2). For the images that are not reflection-symmetric, no axis in the first axes set was found to be a reflection-symmetric axis of the image (case 3).

Case 1: All axes in the first axes are reflection-symmetric axes

For the image given in Fig. 2a1-Fig. 2a4, its first three nonzero GC moments are $GC_{0,1}$, $GC_{0,2}$, and $GC_{0,3}$. The phase of the first nonzero GC moment $GC_{0,1}$ can determine the first axes set $AxesSet_1$, which contains only one axis, shown as a thick gray line in Fig. 2a1. Similarly, the second nonzero GC moment $GC_{0,2}$ can determine two axes in the second axes set $AxesSet_2$, shown as two thin black axes in Fig. 2a2. Notice that the thick gray axis is overlapping with one of these two thin black axes. Finally, the thick gray line is also overlapping with one of the three axes, which are defined by $GC_{0,3}$ and shown as thin black lines in Fig. 2a3. The detected reflection-symmetric axis is shown in Fig. 2a4 by a black line. Similar process is also shown in Fig. 2b, where the image has $GC_{0,2}$, $GC_{0,4}$, and $GC_{0,6}$ as its first three nonzero GC moments.

Case 2: Partial axes in the first axes are reflection-symmetric axes

The image shown in Fig. 3a has the first three nonzero GC moments, $GC_{0,2}$, $GC_{0,3}$, and $GC_{0,4}$. The first axes set $AxesSet_2$ has two axes, shown as two thick gray lines in Fig. 3a1. The second and the third axes sets, $AxesSet_3$ and $AxesSet_4$, respectively, have three and four axes, which are shown as thin black lines in Fig. 3a2 and Fig. 3a3. Notice, only the horizontal axis in Fig. 3a1 has its corresponding one in both Fig. 3a2 and Fig. 3a3. That leads to the correct reflection-symmetric axis shown in Fig. 3a4. Fig. 3b shows the intersection process of the image with the first three nonzero GC moments $GC_{0,4}$, $GC_{0,6}$, and $GC_{0,8}$.

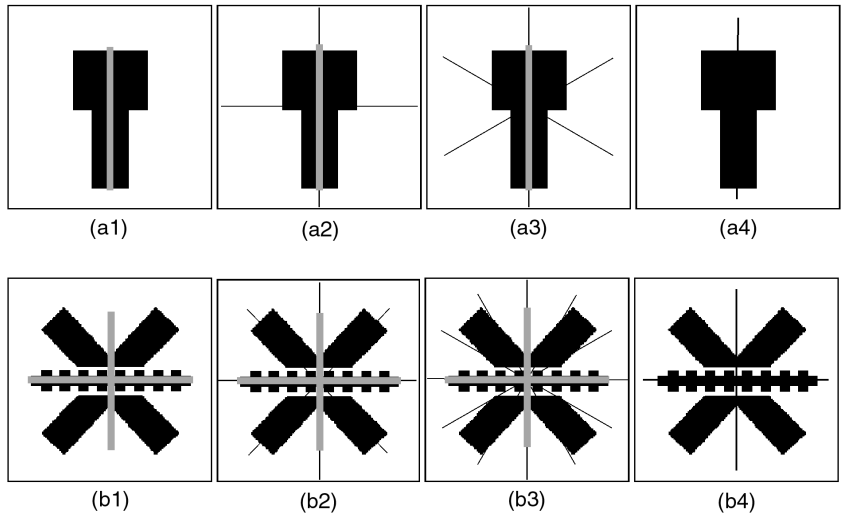

Fig. 2. Two examples of images, whose reflection-symmetric axes are exactly the axes in the first axes set.

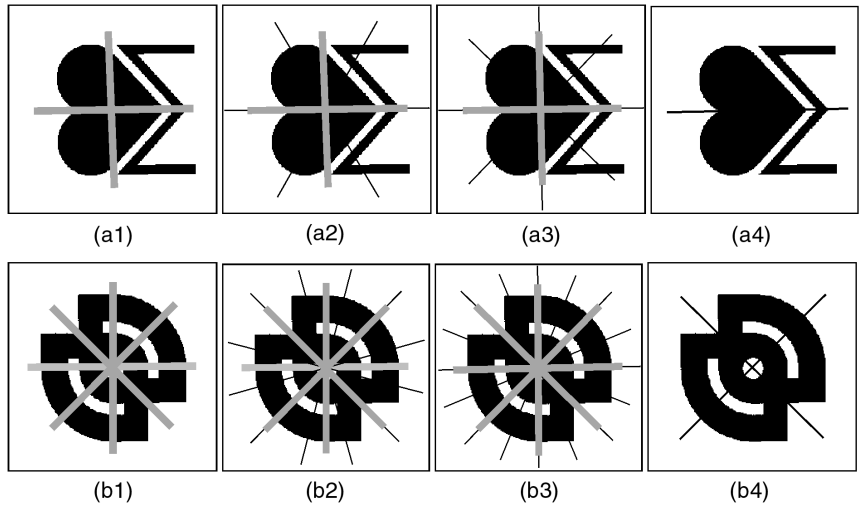

Fig. 3. Two examples showing that only some of the axes in the first axes set $AxesSet_{q_1}$ are the actual reflection-symmetric axes.

Case 3: None of axes in the first axes are reflection-symmetric axes

The first three nonzero GC moments of the image in Fig. 4a are $GC_{6,1}$, $GC_{6,3}$, and $GC_{6,4}$. From Fig. 4a1-Fig. 4a3, none of the axes in the second and the third axes sets, $AxesSet_3$ and $AxesSet_4$, are similar to that of the thick gray line in Fig. 4a1. The result of symmetry detection is that no reflection-symmetric axis exists, that is, the image is not reflection-symmetric. Fig. 4b is another example with the first three nonzero GC moments, $GC_{0,2}$, $GC_{0,4}$, and $GC_{0,6}$. This image is rotationally symmetric, but not reflection-symmetric.

4 Rotational Symmetry Detection

As in the last section, this section will use the same three nonzero GC moments for detecting both the fold number and fold axes of the image.

4.1 Detecting Fold Number

Theorem 2.2 implies that the order q_j in the detected nonzero moment GC_{p,q_j} of a K-RSI should be a multiple of fold number K. Along this line, Theorem 4.1 is inferred for detecting the fold number K of the input image. In practice, the first three nonzero GC moments are enough to detect the fold number of almost every image. That is described in PFND (A Practical Fold Number Detector).

THEOREM 4.1. *Let the detected nonzero GC moments of the given image* $f(r, \theta)$ *be*

$$\{GC_{p,q_j},\ j = 1, 2, 3, \ldots\}.$$

Then the fold number of the image $f(r, \theta)$ *is the biggest common factor of the orders in set* $\{q_j,\ j = 1, 2, 3, \ldots\}$.

PFND: The fold number of *almost every* image $f(r, \theta)$ is the biggest common factor of orders in the set $\{q_1, q_2, q_3\}$, where q_1, q_2, and q_3 are the first three orders making GC moments nonzero,

$$\{GC_{pq_1}, GC_{pq_2}, GC_{pq_3}\}.$$

The first three nonzero moments of the image given in Fig. 2a are $GC_{0,1}$, $GC_{0,2}$, and $GC_{0,3}$. The biggest common factor of these three numbers {1, 2, 3} is 1, which correctly indicates that this

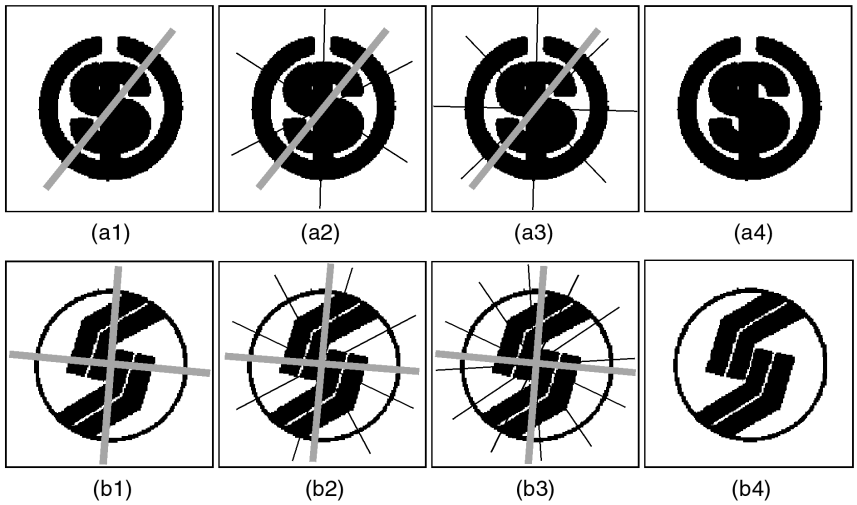

Fig. 4. Two examples showing that no axes in the first axes set $AxesSet_{q_1}$ are the actual reflection-symmetric axes. These images are not reflection-symmetric.

image is a 1-RSI. For another image in Fig. 2b, its first three nonzero GC moments are $GC_{0,2}$, $GC_{0,4}$, and $GC_{0,6}$. The biggest common factor of these three numbers {2, 4, 6} is 2. Thus, the image is a 2-RSI. The other four images in Fig. 3 and Fig. 4 also demonstrate the correctness of PFND.

4.2 Detecting Fold Axes

In rotational symmetry detection, besides detecting the fold number of the input image, detecting its fold axes is also a key problem. Theorem 4.2 gives the method of detecting these fold axes. This theorem also guarantees that the proposed method can define all the fold axes exactly if J is infinite. Theorem 4.2 indicates that, if the number

$$N = \sum_{j=1}^{J} x_j q_j$$

is equal to the biggest common factor of all numbers in set

$$\left\{q_j | j = 1, 2, 3, \ldots J\right\},$$

then the number of half lines, used here to represent the fold axes of image, is equal to the fold number of the image. That is exactly what we need. Theorem 4.3 gives the method for calculating the appropriate integer weights

$$\left\{x_j | j = 1, 2, 3, \ldots J\right\}.$$

Theorems 4.2 and 4.3 are extended from our work in [15]. Again in practice, the first two nonzero GC moments are sufficient for detecting the fold axes. This way, we select $J = 2$ in our experiments.

THEOREM 4.2. *The phase of the combined moment*

$$\prod_{j=1}^{J} (GC_{pq_j})^{x_j}$$

is

$$\sum_{j=1}^{J} x_j \varphi_{pq_j},$$

where GC_{pq_j} $(j = 1, 2, 3, \ldots J)$ *are the detected nonzero GC moments of the input image* $f(r, \theta)$. J *is an integer, and can also be defined infinite.* x_j *is an integer weight. Then there exist*

$$N = \sum_{j=1}^{J} x_j q_j$$

fold axes starting from the origin O and having directional angles

$$\theta_i = \frac{\sum_{j=1}^{J} x_j \varphi_{pq_j} + (i-1) \times 2\pi}{\sum_{j=1}^{J} x_j q_j}$$

with

$$i = 1, 2, \ldots, \sum_{j=1}^{J} x_j q_j.$$

THEOREM 4.3. *There exist appropriate integer weights*

$$\left\{x_j | j = 1, 2, 3, \ldots J\right\}$$

making

$$\sum_{j=1}^{J} x_j q_j$$

equal to the biggest common factor of all orders in

$$\left\{q_j | j = 1, 2, 3, \ldots J\right\}.$$

The appropriate weights

$$\left\{x_j | j = 1, 2, 3, \ldots J\right\}$$

can be obtained by solving the following linear programming problem and selecting the smaller $\left|x_j\right|$ *in the solution set. The objective function is*

$$\min_{\left\{x_j | j=1,2,3,\ldots J\right\}} \sum_{j=1}^{J} x_j q_j,$$

and the constraint conditions are

$$\sum_{j=1}^{J} x_j q_j \geq 1$$

and

$$\left|x_j\right| < \max_{j=1,2,\ldots,J} (q_j).$$

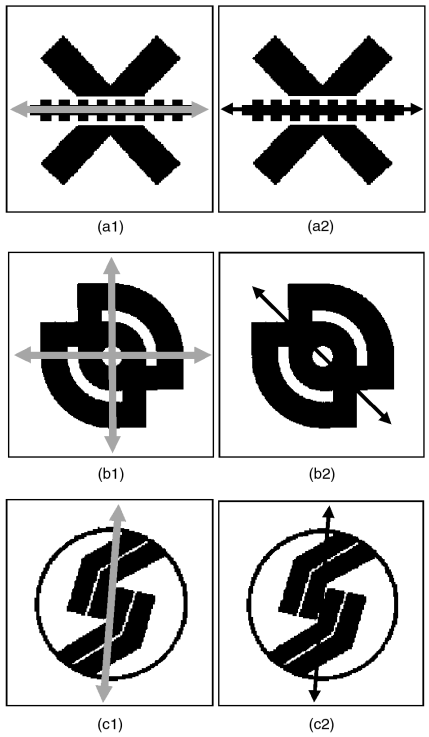

Fig. 5. Compare the fold axes, respectively, defined by the first *one* nonzero GC moment (a1, b1, c1) and the first *two* nonzero GC moments (a2, b2, c2).

After applying the fold number detection algorithm on a set of images, only the images with a fold number bigger than one needs to be processed further for fold axes detection. Images in Fig. 2b, Fig. 3b, and Fig. 4b are now reused as the test images (Fig. 5). If only the first nonzero GC moment GC_{p,q_1} were used to detect the fold axes, we can obtain the fold axes shown as gray arrows in Fig. 5a1, Fig. 5b1, and Fig. 5c1. Notice, the fold axes of Fig. 5a1 and Fig. 5c1 were correctly detected, while the fold axes of Fig. 5b1 were wrongly detected. But using the combined moment of the first two nonzero moments, all the fold axes can be correctly detected (see Fig. 5a2, Fig. 5b2, and Fig. 5c2).

5 Experimental Results and Discussion

A relationship between the number of the reflection-symmetric axes and the number of the fold axes can be derived, based on the notations in [24], [25], for verifying the results of symmetry detection. The relationship is that, for K-RSI($K \geq 1$), the number of the reflection-symmetric axes is either *zero* or K. From this relationship, we can infer that, if the detected number of the reflection-symmetric axes is bigger than *1*, then the image must be rotationally symmetric and its fold number is exactly equal to the detected number of reflection-symmetric axes.

Since the four images in Fig. 2-Fig. 3 are all reflection-symmetric, their numbers of reflection-symmetric axes are equal to the fold numbers. For examples, the image in Fig. 2a has *one* reflection-symmetric axis and its fold number is also *one*. For the other two images in Fig. 4, their numbers of reflection-symmetric axes are both *zeros*.

5.1 A Complete Algorithm for Detecting Reflectional and Rotational Symmetries *(The Shen-Ip Symmetries Detector)*

Since reflectional symmetry detection and rotational symmetry detection use the *same* three nonzero GC moments, the method of detecting symmetries of an image can thus be integrated into a single and efficient algorithm. The *Shen-Ip Symmetries Detector* can be described as follows:

1) Make the input image centered, based on its regular moments.
2) Choose an appropriate p to make the selected 1D function $h_p(\theta)$ having strong alternating energy ($a_p > 5$ percent).
3) Detect first three nonzero GC moments
$$\{GC_{p,q_1}, GC_{p,q_2}, GC_{p,q_3}\},$$
if $b_q \geq 1$ percent and $q \leq 30$ in the process of detecting nonzero GC moments. (The number of nonzero GC moments may be less than three.)
4) Determine reflection-symmetric axes of the image using the phases and orders of the first three GC moments detected,
$$\{GC_{p,q_1}, GC_{p,q_2}, GC_{p,q_3}\} \text{ (PRSD)}.$$
5) Determine the fold number by calculating the biggest common factor of $\{q_1, q_2, q_3\}$(PFND).

If the detected fold number is equal to one, no fold axis exists. Otherwise, use the combined moment of the first two nonzero moments to determine the fold axes of the image. (Theorem 4.2, where $J = 2$.)

5.2 Experiments on Exactly Symmetric Images

To clearly demonstrate the ability of our method, our experimental results are classified into *three* classes:

- Class 1 consists of images whose reflection-symmetric axes are exactly the axes in the first axes set, defined by the first nonzero GC moment.
- Class 2 consists of images, where only some axes in the first axes set are exact ones.
- Class 3 consists of images without any reflection-symmetric axes.

Classifying experiments into three classes do not mean that we need to use different methods for symmetry detection of different images. In fact, we use the same algorithm described above for all the image classes. Additionally, notice that the established relationship between reflectional symmetry and rotational symmetry holds for all the test images in the experiments. The experimental results show that both reflectional symmetry and rotational symmetry of every image in our image database can be detected by our method. There are more than 200 images in the image database.

Class 1: All axes in the first axes set are exactly the reflection-symmetric axes

Some of the images belonging to this class are shown in Fig. 6. The first three nonzero GC moments of every image in Fig. 6 are given in Table 1. Star "*" in the elements of Table 1 means that, under the conditions of the alternating energy limitation and $q \leq 30$, the current nonzero GC moment cannot be detected. For the image with only two nonzero GC moments detected, the process of detecting symmetries is then based on them only. Normally, the process of detecting symmetries of every image is based on the first three nonzero GC moments. Notice that in Fig. 6, every fold axis overlaps with one of the reflection-symmetric axes.

Class 2: Only some of the axes in the first axes set are exactly the reflection-symmetric axes

Fig. 7 shows images, whose actual reflection-symmetric number is less than the order of the first nonzero GC moment. The first three nonzero GC moments, the detected number of reflection-symmetric axes and the fold number of every image in Fig. 7 are shown in Table 2. For example, the first three nonzero GC mo-

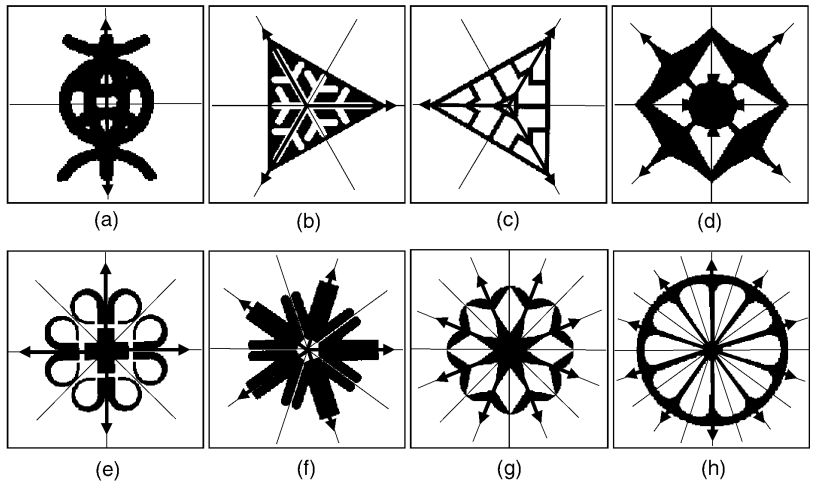

Fig. 6. Experimental results on the images in class 1. In every subfigure, thin lines represent the detected reflection-symmetric axes, while thick arrows denote the detected fold axes.

TABLE 1
THE FIRST THREE DETECTED NONZERO GC MOMENTS, THE DETECTED NUMBER OF REFLECTION-SYMMETRIC AXES, AND THE DETECTED FOLD NUMBER FOR EVERY IMAGE OF CLASS 1 AS SHOWN IN FIG. 6

Non-zero GC moments	figure 6a	Figure 6b	figure 6c	figure 6d	Figure 6e	figure 6f	figure 6g	figure 6h
first one GC_{p,q_1}	$GC_{0,2}$	$GC_{0,3}$	$GC_{0,3}$	$GC_{0,4}$	$GC_{0,4}$	$GC_{0,5}$	$GC_{0,8}$	$GC_{0,10}$
second one GC_{p,q_2}	$GC_{0,6}$	$GC_{0,12}$	$GC_{0,6}$	$GC_{0,8}$	$GC_{0,8}$	$GC_{0,10}$	$GC_{0,24}$	$GC_{0,20}$
third one GC_{p,q_3}	$GC_{0,8}$	$GC_{0,18}$	$GC_{0,9}$	$GC_{0,12}$	$GC_{0,12}$	$GC_{0,20}$	*	$GC_{0,30}$
number of reflection-symmetric axes, fold number	2, 2	3, 3	3, 3	4, 4	4, 4	5, 5	8, 8	10, 10

ments for Fig. 7a are $GC_{0,10}$, $GC_{0,11}$, and $GC_{0,13}$. If using only the first nonzero GC moment $GC_{0,10}$, 10 axes in the first axes set were defined by this moment. However, only one axis in the first axes set is the correct reflection-symmetric axis, others are incorrect. After using all three moments $\{GC_{0,10}, GC_{0,11}, GC_{0,13}\}$, we found the exact reflection-symmetric axis of this image, which is shown as a black line in Fig. 7a. Since the biggest common factor of the three orders {10, 11, 13} is 1, which indicates fold number 1 and thus no fold axis existing. For the other image in Fig. 7g, its first three nonzero GC moments are $GC_{0,6}$, $GC_{0,8}$, and $GC_{0,12}$. The biggest common factor of the three orders {6, 8, 12} is *2*, which indicates this image is a 2-RSI. If only the first nonzero GC moment $GC_{0,6}$ is used, then reflection-symmetric axes, fold number and fold axes cannot be correctly determined. The two fold axes, detected by the first two nonzero GC moments, are shown as two arrows in Fig. 7g.

Class 3: None of the axes in the first axes set are reflection-symmetric axes

Fig. 8 shows eight images, none of them are reflection-symmetric. Fig. 8a to Fig. 8g illustrate that, the images may be rotationally symmetric, but may be not reflection-symmetric. For example, from Table 3, the first three nonzero GC moments of Fig. 8g are $GC_{0,3}$, $GC_{0,6}$, and $GC_{0,9}$, respectively. Its fold number and fold axes were correctly detected, which are shown in Fig. 8g as three arrows. However, the intersection set of the first three axes sets is nil. That means, no reflection-symmetric axis exists for the image.

5.3 Experiments With Almost-Symmetric Images

Since GC moments extract global features of the image, the proposed GC moments-based method is also able to detect the symmetric axes of almost-symmetric images. Table 4 gives the first three nonzero GC moments of every image in Fig. 9. Fig. 9 shows eight almost-symmetric images, and the detected reflection-symmetric axes and fold axes.

5.4 Discussion

In the experiments above, all the test images are actually gray scale images, however they appear to be binary since their gray-level values are close to either black or white. In fact, the proposed techniques are suitable to detecting symmetries for gray scale images. To further illustrates this point, Fig. 10 shows two examples.

Weighting factor (r^p) in the GC moment definition is very important, which makes us select special orders p for special images. For example, $p = 8$ was used for Fig. 7b, $p = 1$ and $p = 3$ were used for Fig. 8c and Fig. 8d, respectively, and $p = 3$ and $p = 1$ were used for Fig. 9f and Fig. 9h, respectively.

Since GC moments are not invariant to affine transform, we first make the affine-transformed object *compact* by using the Compact Algorithm in [15], before applying GC moments to detect its symmetries. Additionally, there exist methods for detecting affine symmetries based on affine-invariant features defined on the contour of the object [26].

Theoretically, our technique is applicable to object with higher degree of symmetries. However, it depends on the resolutions of the image due to the use of global features. For our case, the image size is 128×128 and we can detect the degree of symmetries up to $K = 20$. For our technique, the computation cost is mainly in the calculation of GC moments. No other computation is required besides logical checking. Also, the speed of our technique depends on the images themselves. Simple image needs less time compared with more complex

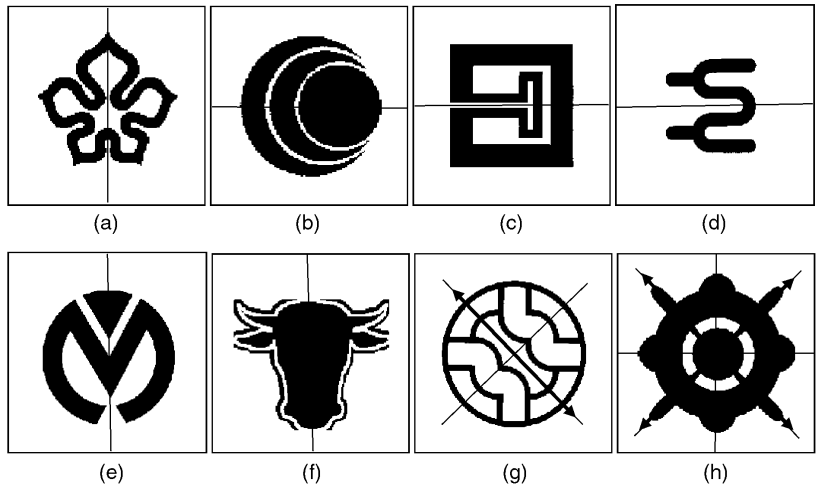

Fig. 7. Experimental results on the images in class 2, where only some of the axes in the first axes set are exactly the reflection-symmetric axes.

TABLE 2
THE FIRST THREE DETECTED NONZERO GC MOMENTS, THE DETECTED NUMBER OF REFLECTION-SYMMETRIC AXES, AND THE DETECTED FOLD NUMBER FOR EVERY IMAGE OF CLASS 1 AS SHOWN IN FIG. 7

Non-zero GC moments	figure 7a	Figure 7b	figure 7c	figure 7d	figure 7e	figure 7f	figure 7g	figure 7h
First one GC_{p,q_1}	$GC_{0,10}$	$GC_{8,3}$	$GC_{0,3}$	$GC_{0,2}$	$GC_{0,5}$	$GC_{0,2}$	$GC_{0,6}$	$GC_{0,8}$
second one GC_{p,q_2}	$GC_{0,11}$	$GC_{8,4}$	$GC_{0,4}$	$GC_{0,3}$	$GC_{0,6}$	$GC_{0,3}$	$GC_{0,8}$	$GC_{0,12}$
third one GC_{p,q_3}	$GC_{0,13}$	$GC_{8,5}$	$GC_{0,12}$	$GC_{0,4}$	$GC_{0,7}$	$GC_{0,5}$	$GC_{0,12}$	$GC_{0,16}$
number of reflection-symmetric axes, fold number	1, 1	1, 1	1, 1	1, 1	1, 1	1, 1	2, 2	4, 4

images. The computation time for calculating one GC moment using a Pentium 233 PC is 0.05 sec.

The robustness of our algorithm against random noises and errors is dependent on the robustness of computing the GC moments in the presence of noises. We have studied the robustness of GC moments computation in the presence of Gaussian noise [15] and shown that GC moments, as global features, are relatively robust to noises. As to uneven lighting effects, i.e., a symmetric object with one side darker than the other side, our technique can endure only a small amonut of nonuniform illuminations due to the use of global features. We have applied our algorithm to the almost-symmetric images, i.e., inexact images, in Subsection 5.3. These examples show that our algorithm can also detect inexact symmetry.

6 CONCLUSION

In this paper, we have presented a unified method for detecting symmetries of every image. Unlike previous approaches that require different methods to detect different types of symmetries, here we combine the detection of both reflectional-symmetry and rotational-symmetry into a single process by using the same set of GC moment features derived from the image. In practice, once the three nonzero GC moments have been calculated, the symmetry axes for reflectional and rotational symmetries can be efficiently determined. We have applied the techniques to over 200 images in our image database. Experimental results show that the proposed method can detect both reflectional symmetry and rotational symmetry of every image. Since GC moments extract global features of the image, our GC moments-based method also has the ability to detect symmetries of almost-symmetric image, even though the image is not exactly symmetric. Furthermore, the derived relationship between reflectional symmetry and rotational symmetry can be used to check the correctness of symmetry detection.

As a conclusion, the main contributions of this paper can be summarized as follows:

1) The reflection-symmetric axes are actually the intersection of all axes sets defined by all the nonzero GC moments.
2) The fold number can be determined by calculating the biggest common factor of all orders making GC moments nonzero.
3) The fold axes can be defined by both the phase and the order of the combined moment, which is generated from all the nonzero GC moments.
4) The relationship between reflectional symmetry and rotational symmetry has been derived.
5) Since GC moments extract global features of the image, the proposed method is able to detect the symmetries of almost-symmetric image.

APPENDIX

The necessary and sufficient condition for $f(r, \theta)$ reflection-symmetric about the x-axis is that all GC moments $GC_{p,q}$ are real.

PROOF.

Necessary: Since x-axis is the reflection-symmetric axis of $f(r, \theta)$, we have $f(r, \theta) = f(r, -\theta)$. This way, we can rearrange $f_m(r)$ as follows:

$$f_m(r) = \frac{1}{2\pi}\int_0^{2\pi} f(r,\theta)e^{jm\theta}d\theta$$

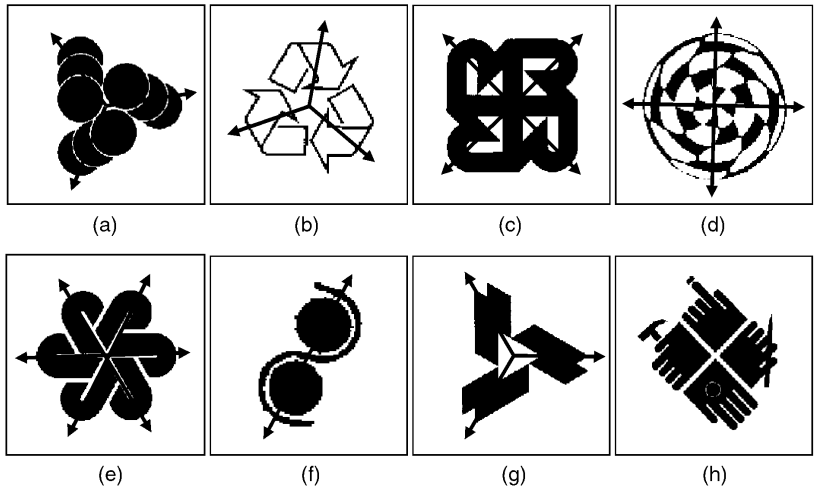

Fig. 8. Experimental results on the images in class 3, where no refection-symmetric axis exists.

TABLE 3
THE FIRST THREE DETECTED NONZERO GC MOMENTS, THE DETECTED NUMBER OF REFLECTION-SYMMETRIC AXES, AND THE DETECTED FOLD NUMBER FOR EVERY IMAGE OF CLASS 1 AS SHOWN IN FIG. 8

Non-zero GC moments	figure 8a	Figure 8b	figure 8c	figure 8d	Figure 8e	figure 8f	figure 8g	figure 8h
First one GC_{p,q_1}	$GC_{0,3}$	$GC_{0,3}$	$GC_{1,4}$	$GC_{3,4}$	$GC_{0,6}$	$GC_{0,2}$	$GC_{0,3}$	$GC_{0,2}$
Second one GC_{p,q_2}	$GC_{0,6}$	$GC_{0,6}$	$GC_{1,8}$	$GC_{3,12}$	$GC_{0,12}$	$GC_{0,4}$	$GC_{0,6}$	$GC_{0,3}$
Third one GC_{p,q_3}	*	$GC_{0,9}$	*	*	*	*	$GC_{0,9}$	$GC_{0,4}$
Number of reflection-symmetric axes, fold number	0, 3	0, 3	0, 4	0, 4	0, 6	0, 2	0, 3	0, 1

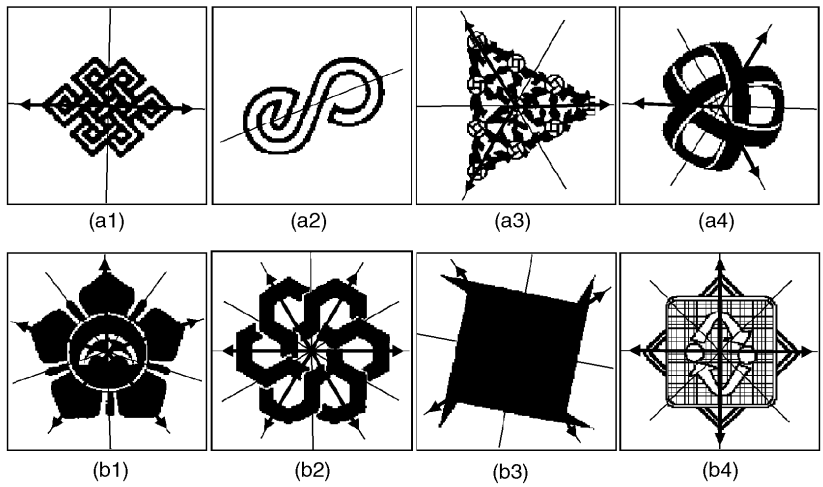

Fig. 9. Symmetry detection on almost-symmetric images.

$$= \frac{1}{2\pi}\int_0^{\pi} f(r,\theta)e^{jm\theta}d\theta + \frac{1}{2\pi}\int_{\pi}^{2\pi} f(r,\theta)e^{jm\theta}d\theta$$

$$= \frac{1}{2\pi}\int_{-\pi}^{0} f(r,\theta)(e^{-jm\theta} + e^{jm\theta})d\theta$$

$$= \frac{1}{2\pi}\int_{-\pi}^{0} f(r,\theta)\cdot 2\cos(m\theta)d\theta\ .$$

The above expansion shows that $f_m(r)$ is real. Additionally, the relationship between GC moment $GC_{p,q}$ and the Fourier coefficient $f_m(r)$ is

$$GC_{p,q} = \int_0^{\infty} f_q(r)r^p r dr\ ,$$

which can be obtained by using the definition of GC moments and the Fourier expansion of image function. Accordingly, all GC moments $GC_{p,q}$ are real because $f_q(r)$ is real.

Sufficient: We can rewrite $f_q(r)$ as

TABLE 4
THE FIRST THREE DETECTED NONZERO GC MOMENTS, THE DETECTED NUMBER OF REFLECTION-SYMMETRIC AXES, AND THE DETECTED FOLD NUMBER FOR EVERY IMAGE OF CLASS 1 AS SHOWN IN FIG. 9

Non-zero GC moments	figure 9a	figure 9b	figure 9c	figure 9d	figure 9e	figure 9f	figure 9g	figure 9h
first one GC_{p,q_1}	$GC_{0,2}$	$GC_{0,2}$	$GC_{0,3}$	$GC_{0,3}$	$GC_{0,5}$	$GC_{3,6}$	$GC_{0,4}$	$GC_{1,4}$
second one GC_{p,q_2}	$GC_{0,4}$	$GC_{0,3}$	$GC_{0,9}$	$GC_{0,6}$	$GC_{0,20}$	$GC_{3,12}$	$GC_{0,8}$	$GC_{1,8}$
Third one GC_{p,q_3}	$GC_{0,6}$	$GC_{0,5}$	$GC_{0,15}$	$GC_{0,9}$	$GC_{0,25}$	*	*	*
Number of reflection-symmetric axes, fold number	2, 2	1, 1	3, 3	3, 3	5, 5	6, 6	4, 4	4, 4

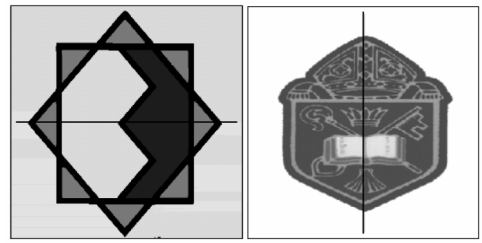

(a) (b)

Fig.10. Symmetry detection on gray scale images.

$$f_q(r) = \mathrm{Re}\left(f_q(r)\right) + j\,\mathrm{Im}\left(f_q(r)\right),$$

where

$$\mathrm{Re}\left(f_q(r)\right) = \frac{1}{2\pi}\int_0^{2\pi} f(r,\,\theta)\cos(q\theta)d\theta,$$

and

$$\mathrm{Im}\left(f_q(r)\right) = \frac{1}{2\pi}\int_0^{2\pi} f(r,\,\theta)\sin(q\theta)d\theta.$$

Since all GC moments are real, then the imaginary parts are zero.

$$\mathrm{Im}(GC_{p,q}) = \int_0^{\infty} \mathrm{Im}\left(f_q(r)\right) r^p dr = 0.$$

The above equation means that all the mapping factors of the function $\mathrm{Im}(f_q(r))$ on r^{p+1} are zeros. To satisfy this requirement, the function $\mathrm{Im}(f_q(r))$ must be zero. That is, $f_q(r)$ is real, which leads to

$$f(r,\theta) = \sum_{m=-\infty}^{\infty} f_m(r)e^{-jm\theta} = \sum_{m=-\infty}^{\infty} f_m(r)\cos(m\theta)$$

and $f(r,\,\theta) = f(r,\,-\theta)$. Therefore, given that all GC moments are real, then the image is reflection-symmetric about the x-axis. □

REFERENCES

[1] J. Ponce, "On Characterizing Ribbons and Finding Skewed Symmetries," *Computer Vision, Graphics, and Image Processing*, vol. 52, pp. 328-340, 1990.

[2] W.G. Oh, M. Asada, and S. Tsuji, "Model-Based Matching Using Skewed Symmetry Information," *Proc. Int'l Conf. Pattern Recognition*, pp. 1,043-1,045, 1988.

[3] D. Reisfeld, H. Wolfson, and Y. Yeshurun, "Robust Detection of Facial Features by Generalized Symmetry," *Proc. Int'l Conf. Pattern Recognition*, pp. 117-120, Champaign, Ill., 1992.

[4] G. Marola, "Using Symmetry for Detecting and Locating Objects in a Picture," *Computer Vision Graphics Image Processing*, vol. 46, pp. 179-195, 1989.

[5] A. Blake, M. Taylor, and A. Cox, "Grasping Visual Symmetry," *Proc. Int'l Conf. Pattern Recognition*, pp. 724-733, 1993.

[6] G. Marola, "On the Detection of the Axes of Symmetry of Symmetric and Almost Symmetric Planar Images," *IEEE Trans. Pattern Analysis and Machine Intelligence*, vol. 11, no. 1, pp. 104-108, 1989.

[7] H. Zabrodsky, S. Peleg, and D. Avnir, "Symmetry as a Continuous Feature," *IEEE Trans. Pattern Analysis and Machine Intelligence*, vol. 17, no. 12, 1995.

[8] M. Atallah, "On Symmetry Detection," *IEEE Trans. Computers*, vol. 34, no. 7, 1985.

[9] T. Masuda, K. Yamamoto, and H. Yamada, "Detection of Partial Symmetry Using Correlation with Rotated-Reflected Images," *Pattern Recognition*, vol. 26, no. 8, 1993.

[10] C. Sun and J. Sherrah, "3D Symmetry Detection Using the Extended Guassian Image," *IEEE Trans. Pattern Analysis and Machine Intelligence*, vol. 19, no. 2, 1997.

[11] F. Labonte, Y. Shapira, and P. Cohen, "A Perceptually Plausible Model for Global Symmetry Detection," *Proc. Fourth Int'l Conf. Computer Vision*, pp. 258-263, 1993.

[12] T. Zielke, M. Brauckmann, and W. V. Seelen, "Intensity and Edge-Based Symmetry Detection with an Application to Car-Following," *Computer Vision, Graphics, and Image Processing: Image Understanding*, vol. 58, no. 2, pp. 177-190, 1993.

[13] S.C. Pei and C.N. Lin, "Normalization of Rotationally Symmetric Shapes for Pattern Recognition," *Pattern Recognition*, vol. 25, no. 9, pp. 913-920, 1992.

[14] J.C. Lin, W.H. Tsai, and J.A. Chen, "Detecting Number of Folds by a Simple Mathematical Property," *Pattern Recognition Letters*, vol. 15, pp. 1,081-1,088, 1994.

[15] D. Shen and H.H.S. Ip, "Generalized Affine Invariant Image Normalization," *IEEE Trans. Pattern Analysis and Machine Intelligence*, vol. 19, no. 5, pp. 431-440, May 1997.

[16] D. Shen and H.H.S. Ip, "Optimal Axes for Defining the Orientations of Shapes," *IEE Electronic Letters*, vol. 32, no. 20, pp. 1,873-1,874, Sept. 1996.

[17] C. Sun, "Fast Recovery of Rotational Symmetry Parameters Using Gradient Orientation," *SPIE J. Optical Eng.*, vol. 36, no. 4, pp. 1,073-1,077, 1997.

[18] W.H. Tsai and S.L. Chou, "Detection of Generalized Principal Axes in Rotationally Symmetric Shapes," *Pattern Recognition*, vol. 24, pp. 95-104, 1991.

[19] S.L. Chou, J.C. Lin, and W.H. Tsai, "Fold Principal Axis—A New Tool for Defining the Orientations of Rotationally Symmetric Shapes," *Pattern Recognition Letters*, vol. 12, pp. 109-115, 1991.

[20] J.C. Lin, "Universal Principal Axes: An Easy-to-Construct Tool Useful in Defining Shape Orientations for Almost Every Kind of Shape," *Pattern Recognition*, vol. 26, no. 4, pp. 485-493, 1993.

[21] D. Shen and H.H.S. Ip, "Discriminative Wavelet Shape Descriptors for Recognition of 2D Patterns," *Pattern Recognition*, vol. 32, no. 2, pp. 151-166, Feb. 1999.

[22] M.K. Hu, "Visual Pattern Recognition by Moment Invariants," *IRE Trans. Information Theory*, vol. 8, 179-187, 1962.
[23] J. Bigun and J.M.H. du Buf, "N-Folded Symmetries by Complex Moments in Gabor Space and their Application to Unsupervised Texture Segmentation," *IEEE Trans. Pattern Analysis and Machine Intelligence*, vol. 16, no. 1, pp. 80-87, 1994.
[24] H. Wely, *Symmetry*, Princeton Univ. Press, 1952.
[25] W. Miller, *Symmetry Groups and their Application*, Academic Press, 1972.
[26] D. Shen, H.H.S. Ip, and E.K. Teoh, "Robust Detection of Skewed Symmetries by Combining Local and Semi-Local Affine Invariants," *IEEE Trans. Pattern Analysis and Machine Intelligence*, submitted for publication.
[27] H.H.S. Ip, D. Shen, and K.K.T. Cheung, "Indexing and Retrieval of Binary Patterns Using Generalized Complex Moments," *Proc. Second Int'l Conf. Visual Information System*, California, Mar. 1997.
[28] C. Sun, "Symmetry Detection Using Gradient Information," *Pattern Recognition Letters*, vol. 16, no. 9, pp. 987-996, 1995.